LA-UR- 10-07530

Approved for public release; distribution is unlimited.

Title:	Modal Analysis and SHM Investigation of CX-100 Wind Turbine Blade
Author(s):	Krystal E. Deins, INST-OFF, LANL Timothy (NMI) Marinone, INST-OFF, LANL Ryan A. Schultz, INST-OFF, LANL Kevin M. Farinholt, AET-1 LANL Gyuhae (NMI) Park, INST-OFF, LANL
Intended for:	IMAC XXIX A CONFERENCE AND EXPOSITION ON STRUCTURAL DYNAMICS, Jacksonville, FL, January 31-February 3, 2011.

Los Alamos
NATIONAL LABORATORY
EST. 1943

Form 836 (7/06)

Modal Analysis and SHM Investigation of CX-100 Wind Turbine Blade

Krystal Deines[1], Timothy Marinone[2], Ryan Schultz[3], Kevin Farinholt[4], Gyuhae Park[4]

1. Dept. of Aerospace Eng., New Mexico State University, Las Cruces, NM, 88003
2. Dept. of Mechanical Eng., University of Massachusetts Lowell, Lowell, MA 01854
3. Dept. of Mechanical Eng., Michigan Technological University, Houghton, MI 49931
4. The Engineering Institute, Los Alamos National Laboratory, Los Alamos, NM 87545

Abstract

This paper presents the dynamic characterization of a CX-100 wind turbine blade using modal testing. Obtaining a thorough dynamic characterization of turbine blades is important because they are complex structures, making them very difficult to accurately model without supplementing with experimental data. The results of this dynamic characterization can be used to validate a numerical model and understand the effect of structural damage on the performance of the blades. Also covered is an exploration into Structural Health Monitoring (SHM) techniques employed on the blade surface to detect changes in the blade dynamic properties. SHM design parameters such as traveling distance of the wave were examined. Results obtained during modal and SHM testing will provide a baseline for future work in blade damage detection and mitigation.

1.0 Introduction

1.1 Background

Wind energy in the United States is the fastest growing source of renewable domestic energy. A recent DOE technical report [1] proposed the potential for meeting 20% of the nation's energy needs through wind power by 2030. This significant investment in wind turbines is motivating manufacturers to produce more efficient and therefore larger and more complex wind turbines. The trend in wind energy is also toward larger, longer, yet lighter blades in order to generate more power. Significant effort is being expended in order to improve the design and manufacturability of the blades [2, 3, 4].

Maximizing the reliability of wind turbine design is a key to providing safe and cost effective operation. Monitoring the structural health of the turbine blades is particularly important as they account for 15-20% of the total turbine cost. In addition, blade damage is the most expensive type of damage to repair and can cause serious secondary damage to the wind turbine system due to rotating imbalance created during blade failure. Accurate assessment of blade structural health is critical financially as wind turbines are often in remote locations, and require substantial time, effort and cost to repair if failed [5]. If predictive maintenance can be employed, that could mean a substantial reduction in downtime which readily translates to significant cost savings for the wind farm operator.

1.2 Previous Work

Modal analysis of a CX-100 wind turbine blade in a free-free configuration and attached to a Micon 65/13 Wind Turbine by White et al. [6] determined that boundary condition supports affected the frequencies and mode shapes. Modal analysis of a Blade System Design Study (BSDS) blade by Griffith et al. [7] demonstrated a unique boundary condition approach by attaching the blade to a seismic mass and airbag assembly in a vertical orientation. Fatigue testing of a TX-100 blade with SHM by Rumsey et al. [8] determined that failure occurred at the out-board blade spar-cap termination point at 4.5 meters from the root.

A review of various SHM techniques was described by Ciang et al. [9], which compared the techniques for detecting localized vs. global damage along with the number of sensors needed and potential issues with each technique. Evaluation of three SHM techniques: Lamb wave, frequency response, and time series were performed by Light-Marquez et al. [10] showing the advantages and disadvantages of each technique.

1.3 Purpose

The purpose of this study is to characterize the dynamic response of the CX-100 wind blade and the design parameters of SHM techniques as they apply to the wind turbine blade. An examination of boundary conditions in both a free-free and fixed-free configuration will be investigated. This characterization will serve as a baseline for further work as well as validate developed dynamic models. Also explored is the usable frequency range for MFC patch sensors located on the spar at various span-wise locations along the length of the blade.

2.0 Experimental Procedure

2.1 Pre-Test Setup

A grid was created on the blade's high and low pressure surfaces for measurement location reference. This grid was aligned on the X, Y and Z axes of the CX-100 CAD model. As such, all measurement locations can be easily translated from a point on the complex surface of the blade to a point in the X, Y, and Z coordinate system of the model. The grid has points every 0.5 meters along the blade length and every 0.2 meters along the blade chord, Figure 1.

Figure 1: Measurement location grid on CX-100

2.2 Free-Free Modal Test I

Due to data collection limitations, a roving hammer test was used, employing three shear accelerometers (PCB 352C22) and a modal impact hammer (PCB 086D20). Preliminary testing determined the required sensitivity and location of each accelerometer on the blade. The low-pressure surface was selected as the impacting and measuring surface as flap-wise modes were of primary interest. In addition, the low-pressure surface has less curvature than the high-pressure surface. Accelerometer locations are shown in Figure 2. The impact hammer tip was selected to excite up to 150Hz which contains the first several modes.

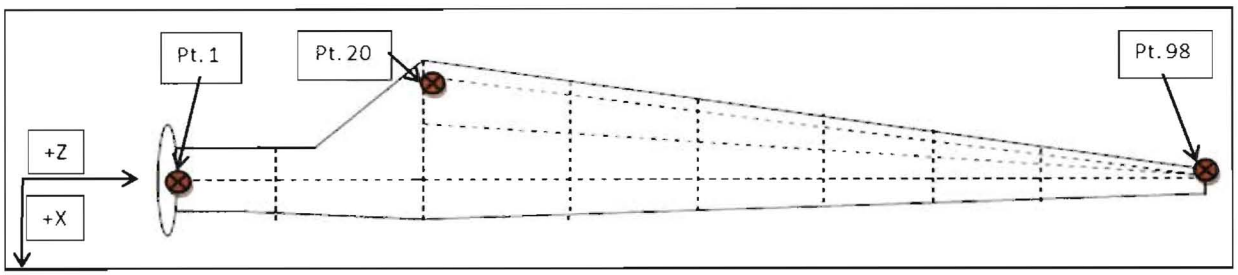

Figure 2: Accelerometer locations on blade low-pressure surface

The blade was suspended from metal frames by way of lifting sling support straps at two points. The tip-end support strap was placed at the node of the first flap-wise bending mode which was located during preliminary testing, Figure 3. In all tests, the response of the frames was characterized by instrumenting with accelerometers and impacting at various points to determine any coupling of frame and blade modes.

Figure 3: CX-100 in Free-Free I configuration

In order to minimize the effects of the boundary conditions (support straps) on the frequency and mode shape, the support strap was place at the node of the first mode. The blade was impacted at several points along the length and chord of the blade in the flap-wise direction, taking care to measure and impact on the Y-Z plane.
RT Dactron was used for collection of data which was output in UFF files, while ME'scope was used for curve-fitting and analysis. The data collection parameters used can be seen in Table 1.

Table 1: Modal Tests Data Collection Parameters

Sampling Frequency (Hz)	150
Number of Data Points	4096
Number of Averages	5
Sampling Time (s)	11
Type of Average	Linear
Window	None

2.2.1 Boundary Condition Study of Free-Free Modal Test I

To determine the effects of various boundary conditions on the blade response, a boundary condition study was performed. By changing one aspect of the blade boundary conditions at a time, measuring the response and comparing with a baseline measurement, the effects were quantified. Boundary conditions examined were the Z location of the support straps (both root and tip-ends), the angle of the blade in the support straps (rotating

about the length) which changes the contact of the straps with the blade surface, and the stiffness of the metal support frames. The blade was impacted and measured at the three drive points (1, 20 and 98), Figure 2.

2.3 Free-Free Modal Test II

To create strain energy in the root of the blade that was absent in the first free-free test, a large mass was bolted to the root. This mass is the top of the fixture used in fixed-free testing (section 2.4) and weighs approximately 500lbf. To approach a free-free condition with this new setup, the fixture was set on wood blocks covered in carpet, leaving the root end with the fixture free to move. The tip-end was then supported with a support strap to keep the blade from tipping, Figure 4. The same impact and measuring process as the Free-Free Modal Test I was used. As in Free-Free Modal Test I, a characterization of the fixture was performed.

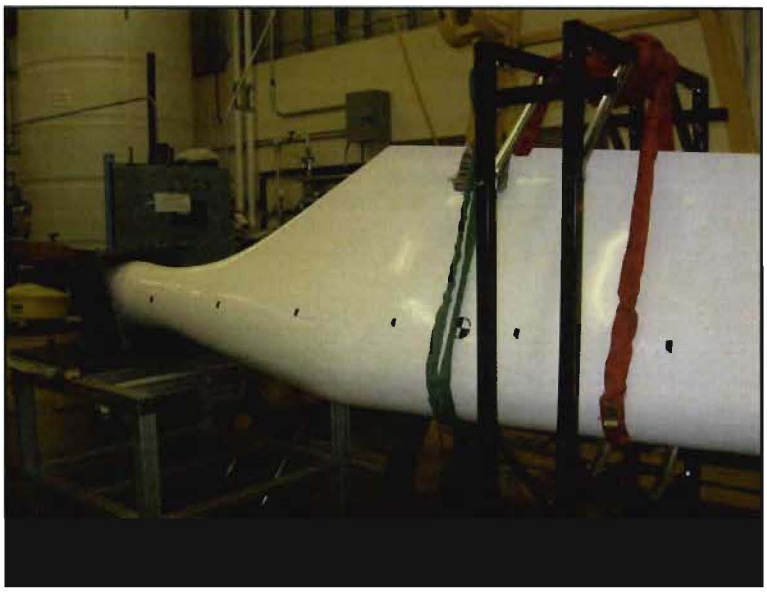

Figure 4: Free-Free Modal Test II setup with fixture bolted to blade root

2.4 Fixed-Free Modal Test

Modal testing of the blade was also performed with a fixed-free condition by bolting the blade to a metal fixture in a cantilevered configuration. The blade was oriented with the chord at the tip vertical, as in the free-free tests.

Modal testing was performed using the same procedure as described in 2.2, using the same accelerometers and roving hammer technique to measure the flap-wise response. Next, accelerometers were placed on the trailing edge of the blade and oriented with the blade's X-axis to measure lead-lag modes. The blade was impacted along the leading edge with the same impact hammer to excite these lead-lag modes.

The fixture is not perfectly rigid and therefore not a truly fixed condition. To account for the effects of the fixture on the blade response, accelerometers were added to various locations on the fixture to characterize its response due to impacts on the blade and on the fixture.

Figure 5: Blade mounted to fixture for Fixed-Free Test

2.5 Structural Health Monitoring

An exploratory investigation into the application of structural health monitoring techniques on the full CX-100 blade was performed. The blade was bolted to the fixture as in the Fixed-Free Modal Test. The aim was to apply one large actuation macro-fiber composite (MFC) patch to the blade high-pressure surface and then detect the applied signals with several smaller sensor MFC patches placed along the length of the blade. The actuation patch is from www.smart-material.com, type 15B10-0211 and located on the X=0 centerline, which is also where the spar-cap is located, two meters from the root end (point three in Figure 6) below. The sensor patches are also from www.smart-material.com, type 20E10 and located per Figure 6.

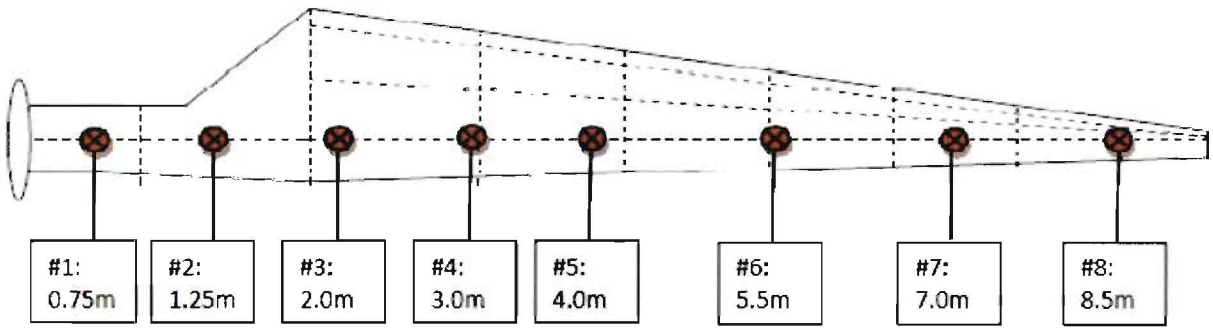

Figure 6: Sensor MFC patch locations on blade centerline

As can be seen in Figure 6, sensor patches were concentrated toward the root, because the transition region from structural to aerodynamic (near the root) is the region where failure typically occurs.

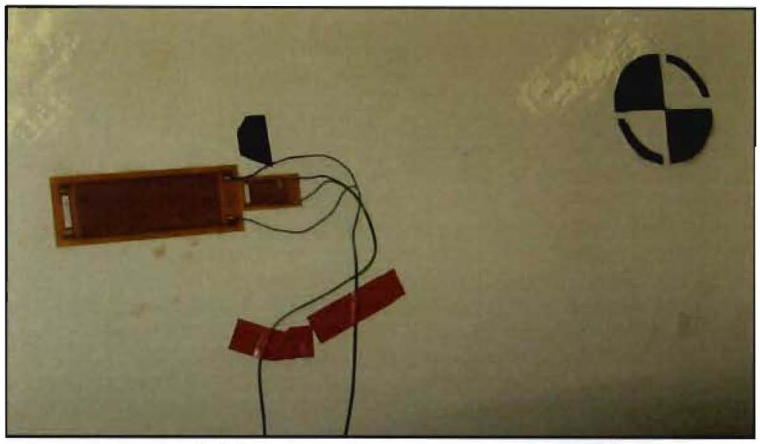

Figure 7: Large actuator MFC (left) and small sensing MFC (right) at point 3 near CG of CX-100

In this experiment, eight small MFC patches were used as sensing patches and one larger patch was used as an actuator. One sensing patch was placed immediately next to the actuating patch to read the strain output in the area close to the actuation patch, Figure 7. Two excitation signals were used - sine chirp and burst random. A shear accelerometer (PCB 352C22, 100mV/g) was placed at the sensing MFC patch during each test for comparison of the observed signals in the frequency range of the accelerometer. An amplifier, AV Power Series 790, was used with the actuator patch to produce enough energy in the blade for the sensor patches to read.

3.0 Data Analysis

3.1 Free-Free Modal Test I

A modal test of the blade in a free-free configuration was performed as described in 2.2. Me'scope was used to curve fit the frequency response data and estimate natural frequencies, damping ratios, and mode shapes. The results are shown in Table 2.

Table 2: Modal Results for CX-100 Rotor Blade with Free-Free I Boundary Condition

Mode	Frequency (Hz)	Damping (% critical)	Description
1	7.61	0.195	1st Flap Bending
2	18.1	2.960	1st Lag Bending
3	20.2	0.752	2nd Flap Bending
4	32.2	0.353	3rd Flap Bending
5	45.1	0.733	2nd Lag Bending
6	50.5	0.630	4th Flap Bending
7	63.9	0.740	1st Torsion
8	70.1	0.568	3rd Lag Bending

3.1.1 Boundary Condition Study of Free-Free Modal Test I

From previous literature [12], the boundary condition in a free-free configuration was found to have an effect on the natural frequencies and mode shapes observed. In order to determine the effect of the boundary conditions on the response, a boundary condition study was performed by varying the boundary condition and comparing the resultant FRFs.

Table 3 is a summary of the different conditions tested with the average percent difference from the baseline for the first three flap-wise modes. The baseline test included a strap support at the root end and a strap support with standard metal frames at the node of the first flap-wise mode. The chord was oriented parallel to gravity. Details are in Appendix A.

Table 3: Summary of Boundary Condition Effects

Boundary Configuration	Percent Difference
Lifting the Blade	0.00
Rotation of the Blade	1.01
Attaching Angle Brackets to Unistrut Frame	1.67
Stiffened Frame Moved Out Toward Tip	8.20
Stiffened Frame Moved Slightly Inward	4.40
Stiffened Frame Moved to Center of Gravity	3.81
Percent of Support in Contact with Blade	2.87
Root Support Moved Slightly Outward	2.36

Overall, the boundary condition changes had an effect on the frequencies of the first mode. However, some boundary condition changes had greater effects on the first mode frequency than others, especially the shift of the tip-end support.

3.2 Free-Free Modal Test II

A modal test of the blade in the Free-Free II configuration was performed as described in 2.3. In order to ensure safety, an additional support needed to be located at the CG. Two configurations were examined: hanging the blade from Unistrut frame with a sling, and placing a cart with packing foam underneath, Figure 8.

Table 4 contains a comparison of the frequencies for both configurations.

Figure 8: Free-Free II configuration with cart and packing foam supporting blade

Table 4: Comparison of Natural Frequencies for Free-Free II

Mode	Unistrut Configuration (Hz)	Packing Foam Platform Configuration (Hz)	Percent Difference
1st Flap-wise	3.29	2.93	10.94
2nd Flap-wise	8.72	8.97	2.79
3rd Flap-wise	17.60	17.40	1.14
4th Flap-wise	30.70	30.00	2.28
5th Flap-wise	45.00	42.30	6.00
1st Torsion	50.90	54.90	7.29

As with Free-Free I, boundary conditions have an effect on the blade response, shown in Table 4.

3.2.1 Nonlinear Study

A significant assumption during modal testing is system linearity, which allows the complete FRF matrix to be created from a subset of the data. In order to determine if the linearity assumption was valid for the blade and boundary condition system, two tests were performed on the system. The first test involved impacting the same location at different force amplitudes and comparing the resulting FRFs. The second test involved a reciprocity check by impacting and measuring at two points, and overlaying the FRFs. From the study, system nonlinearity was observed, but was found to have negligible effect on the resonant frequencies identified within a given input force range of interest. Thus, the linear assumption was deemed valid for the purpose of testing. Further details of the test can be found in Appendix B.

3.3 Fixed-Free Modal Test

A modal test of the blade in a Fixed-Free configuration was performed, as described in 2.4. The results are shown in Table 5.

Table 5: Modal Results for CX-100 Rotor Blade with Free-Fixed Boundary Condition

Mode	Frequency (Hz)	Damping (% critical)	Description
1	3.22	0.203	1st Flap Bending
2	4.15	0.250	1st Lag Bending
3	8.81	0.245	2nd Flap Bending
4	16.80	0.306	2nd Lag Bending
5	19.20	0.345	3rd Flap Bending
6	30.80	0.263	4th Flap Bending
7	37.20	0.789	3rd Lag Bending
8	43.90	0.499	1st Torsion

Testing in the Fixed-Free configuration resulted in lower blade natural frequencies than either free-free test. In addition, the natural frequencies obtained from attaching the fixture to the blade in the free-free configuration are very similar to the natural frequencies obtained in the fixed-free configuration. This shows that the additional effect of the stiffness of the fixture attached to the frame is minimal compared to the effect of adding the fixture onto the blade.

3.4 Structural Health Monitoring

SHM tests of the blade were performed as described in 2.5. Examination of the responses at the 8 points showed an effective frequency range that is listed in Table 6.

Table 6: Effective Frequency for Points on Blade

Point	1	2	3	4	5	6	7	8
Effective Frequency (kHz)	0-20	0-20	0-20	0-20	5-20	5-20	5-20	5-20

Locations in the structural region near the root exhibit noticeable responses across the entire frequency range, showing that SHM could be effective for the region. In contrast, locations in the aerodynamic region toward the tip exhibit a markedly decreased response across a smaller frequency range, indicating that SHM may not be as effective for that region. Further details of the test can be found in Appendix C.

4.0 Conclusions

Modal testing of a 9 meter CX-100 wind turbine blade was performed in both free-free and free-fixed configuration and the natural frequencies and mode shapes were obtained for the first several modes. A study of the effect of the boundary conditions on a free-free configuration was also performed, showing that the supports have a nontrivial effect on the blade response. MFC sensor patches were applied to the structure to determine the effective frequency range at various points along the blade. Greater signal attenuation existed in the aerodynamic region of the blade as compared to the structural region.

Modal analysis of the fixed-free configuration showed that the fixture and frame did not provide a perfectly fixed condition, which resulted in noticeable motion of the fixture and frame coupled with the blade. Accordingly, another modal test of the blade should be performed with the blade attached to a large seismic mass with greater mass and inertia (like that at the National Renewable Energy Laboratory) in order to truly replicate a fixed boundary condition. Damage could not be induced in the blade due to need for further study of the blade in good condition. Accordingly, SHM testing of a blade with damage or simulated damage should be performed to determine the effectiveness in detecting damage in the structural region. The effect of the placement of the patches should also be studied to optimize their location.

5.0 Acknowledgements

All of this work was made possible by the Los Alamos National Laboratory Engineering Institute under the leadership of Dr. Chuck Farrar, which provided the blade and all the equipment used. Vibrant Technology Inc. graciously provided the license for ME'scope software which was used for all data analysis. ABAQUS graciously provided a license for their software which was used for analysis of the fixture support. Lastly, Dr. Peter Avitabile (University of Massachusetts Lowell) provided invaluable guidance over the course of this project.

6.0 References

1. U.S. Department of Energy. "20% Wind Energy by 2030." July 2008
2. TPI Composites, Inc., "Innovative Design Approaches for Large Wind Turbine Blades," Project Report for SNL, SAND2003-0723, March 2003.
3. TPI Composites, "Innovative Design Approaches for Large Wind Turbine Blades; Final Report", SAND2004-0074, Sandia National Laboratories, Albuquerque, NM
4. Ashwill, T.D., "Some Recent Trends & Activities in Turbines and Blades," Sandia National Laboratories 2nd Wind Turbine Blade Workshop, April 2006.
5. JÜNGERT, ANNE. "Damage Detection in Wind Turbine Blades using two Different Acoustic Techniques", 7th PhD Symposium in Stuttgart, Germany, September 11 – 13, 2008
6. White, J.R., Adams, D.E., Rumsey, M.A., "Modal Analysis of CX-100 Rotor Blade and Micon 65/13 Wind Turbine", Proceedings of the IMAC-XXVII, Feb. 1-4, 2010, Jacksonville, FL
7. Griffith, D.T., Carne, T.G., "Experimental Modal Analysis of 9-meter Research-sized Wind Turbine Blades", Proceedings of the IMAC-XXVII, Feb.1-4, 2010, Jacksonville, FL
8. Rumsey, M.A., Paquette, J.A., "Structural Health Monitoring of Wind Turbine Blades" , Sandia National Laboratories, Albuquerque, NM
9. Ciang, C.C., Lee, J.R., Bang, H.J., "Structural Health Monitoring for a Wind Turbine System: A review of Damage Detection Method," Meas. Sci. Technol. 19 (2008), 122001.
10. Light-Marquez, A., Sobin, A., Park, G., Farinholt, K., "Structural Damage Identification in Wind Turbine Blades using Piezoelectric Active-sensing," Proceedings of the IMAC XXVIII, Feb. 1-4, 2010, Jacksonville, FL.
11. Griffith, D.T., Carne, T.G., Paquette, J.A., "Modal Testing for Validation of Blade Models", Wind Engineering Vol. 32, No. 2, 2008, PP 91–102, Sandia National Laboratories, Albuquerque, New Mexico

Appendix A: Boundary Condition Study

In order to determine the effect of the boundary conditions on the free-free mode shapes and frequencies, testing of the blade was performed with several variations in the boundary conditions. A drive point measurement at the tip was used as a baseline FRF for comparison with the effect of the other conditions.

Test 1: Lifting of the Blade

Before going into any further study of the boundary conditions, there is a need to know if the measurement was repeatable without any boundary condition change. Accordingly, the tip end of the blade was lifted up out of the tip end support sling and set back down in the original position. The resulting FRF overlay is shown in Figure 9, where the black trace is the baseline measurement, and the red trace is the measurement after lifting and returning the blade in the support sling.

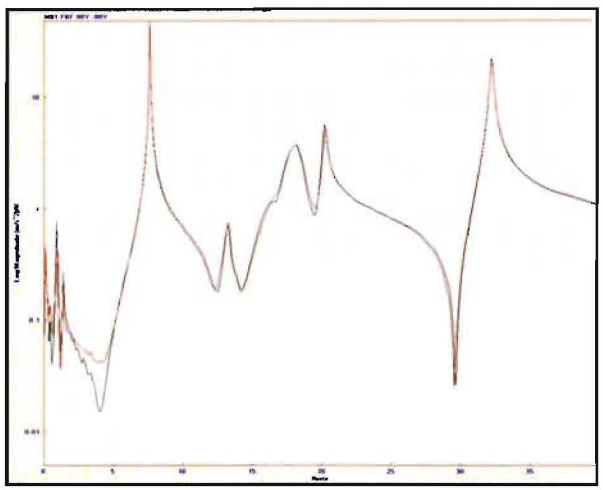

Figure 9: FRF comparison between baseline (black) and lifted (red) configurations

For the uses of this experiment, the frequency range of interest contains the first three flap-wise modes; zero to 40 Hz. Comparison of the two FRFs shows negligible difference between the two measurements in the frequency range of interest. In both frequency and amplitude, the FRFs are almost perfect replicas of each other, especially in the first three flap-wise modes. Table 7 is a comparison of the frequencies for the first three flap-wise modes.

Table 7: Comparison of Natural Frequencies for the Baseline and Lifted Configuration

	Baseline Configuration (Hz)	Lifted Configuration (Hz)	Percent Difference
First Flap-wise	7.6	7.6	0
Second Flap-wise	20.2	20.2	0
Third Flap-wise	32.2	32.2	0

Test 2: Rotation of the Blade

The initial orientation of the blade was such that the chord at the tip was parallel to gravity in an attempt to maximize the response of the flap-wise modes. Since a true free-free configuration would produce the same modes regardless of the angle of orientation, the blade was rotated 12° clockwise to determine the effect of changing the contact areas of the tip end support sling, Figure 10. The resulting FRF overlay is shown in Figure 11, where the black trace is the baseline measurement, and the red trace is the measurement after rotating the blade.

Figure 10: Blade in baseline orientation (left) versus rotated 12° orientation (right)

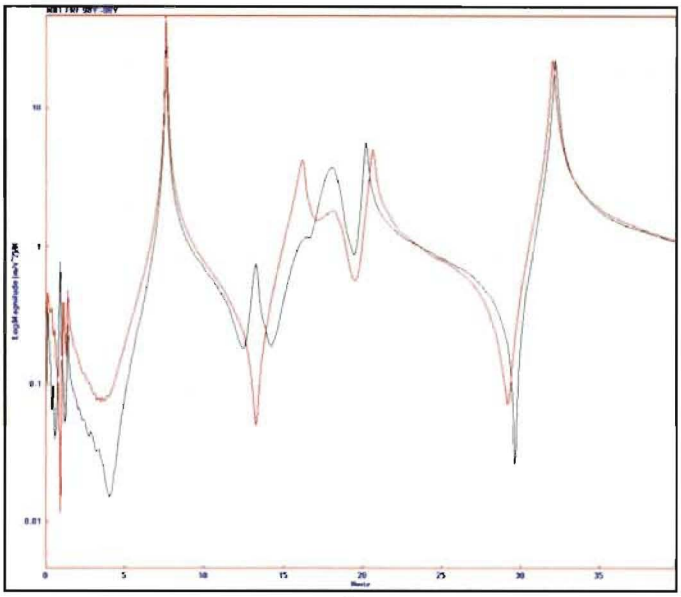

Figure 11: FRF comparison between baseline and rotated configurations

Comparison of the two FRFs shows minimal difference at the first and third flap-wise modes, but a noticeable difference at the second flap-wise mode. A possible explanation for this difference is a change in the interaction of the second flap-wise mode with the first lead-lag mode, which occurs at 18 Hz. Adjusting the rotation may cause the lead-lag mode to have a larger amplitude, affecting the frequency of the second flap-wise-mode. Table 8 is a comparison of the frequencies for the first three flap-wise modes.

Table 8: Comparison of Natural Frequencies for the Baseline and Rotated Configurations

	Baseline Configuration (Hz)	Rotated Configuration (Hz)	Percent Difference
First Flap-wise	7.6	7.6	0
Second Flap-wise	20.2	20.7	2.42
Third Flap-wise	32.2	32.0	0.62

Test 3: Stiffening the Unistrut Frame

The original supports for the blade consisted of two Unistrut frames, one supporting the tip end and one supporting the root end. Testing of the tip end frame revealed a shearing mode at 8.1 Hz, close to the first natural frequency of the blade, 7.61 Hz. In order to determine if there was a coupling effect between the frame

and the blade, the frame stiffness was increased by adding angle brackets to the corners to shift the natural frequency out of the range of the blade's first flap-wise mode, Figure 12. The resulting FRF overlay is shown in Figure 13, where the black trace is the baseline measurement, and the red trace is the measurement after adding the angle brackets.

Figure 12: Frame in baseline configuration (left) versus the stiffened frame (right)

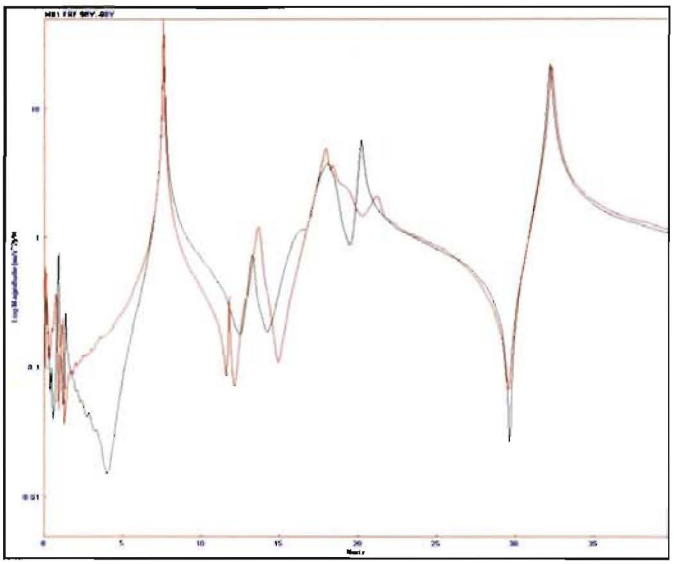

Figure 13: FRF Comparison between baseline (black) and stiffened frame Unistrut (red) configurations

Comparison of the two FRFs shows minimal difference at the first and third flap-wise modes, but a noticeable difference at the second flap-wise mode. A possible explanation for this difference is due to the change in frequency caused by the stiffened frames changing the interaction of the frame with the blade at that frequency. Modal analysis of the stiffened frame yielded a shearing mode at 18.1 Hz, which may couple with the second flap-wise blade mode and alter the measured frequency. Table 9 is a comparison of the frequencies for the first three flap-wise modes.

Table 9: Comparison of Natural Frequencies for the Baseline and Stiffened Frame Configurations

	Baseline Configuration (Hz)	Stiffened Frame Configuration (Hz)	Percent Difference
First Flap-wise	7.6	7.6	0
Second Flap-wise	20.2	21.2	4.72
Third Flap-wise	32.2	32.3	0.31

Test 4: Stiffened Tip-End Frame Moved to 8 Meters from Root

Previous research had shown that the location of the supports had an effect on the natural frequencies obtained [11]. As such, the tip-end support was located at the node of the first flap-wise bending mode (6.518m from root) to minimize the effect of that support on that mode. To quantify the effect of support location on the frequencies and mode shapes, the tip-end support was moved outboard toward the tip (8m from root), Figure 14. The resulting FRF overlay is shown in Figure 15. All supports were stiffened with brackets.

Figure 14: Tip-end frame in baseline location 6.5m from root (left) versus moving the frame to 8m from root (right)

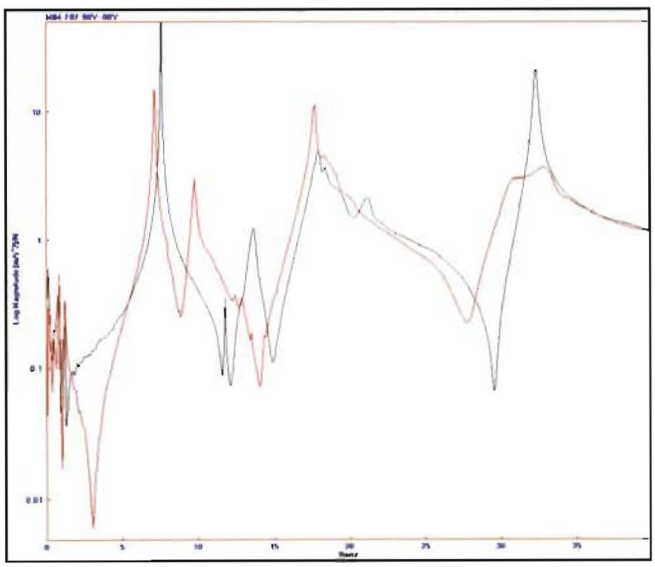

Figure 15: FRF comparison between stiffened baseline (black) and stiffened tip 8 meter (red) configurations

Comparison of the two FRFs shows noticeable difference at all three modes. This is due to relocating the added stiffness of the support (tip-end frame) to a new location on the blade that exhibits greater response, thereby magnifying the effect of the boundary condition. Changing the support location alters the system stiffness and

therefore changes the frequencies and mode shapes. Table 10 is a comparison of the frequencies for the first three flap-wise modes.

Table 10: Comparison of Natural Frequencies for the Stiffened Baseline and Tip Support Configuration Stiffened 8 Meter Configurations

	Stiffened Baseline Configuration (Hz)	Stiffened 8 Meter Configuration (Hz)	Percent Difference
First Flap-wise	7.6	7.14	6.05
Second Flap-wise	21.2	17.7	16.51
Third Flap-wise	32.3	33.0	2.12

Test 5: Stiffened Tip End Frame Moved to 5 Meters from Root

Although moving the frame out to the tip showed significant change, that location would generally not be chosen for testing because the tip has the response with the greatest magnitude. To test the effect of locating a support near the node of the first flap-wise mode, the tip-end frame was placed 5 meters from the root end, Figure 16. The resulting FRF overlay is shown in Figure 17.

Figure 16: Tip-end frame in baseline location 6.5m from root (left) versus moving the frame to 5m from root (right)

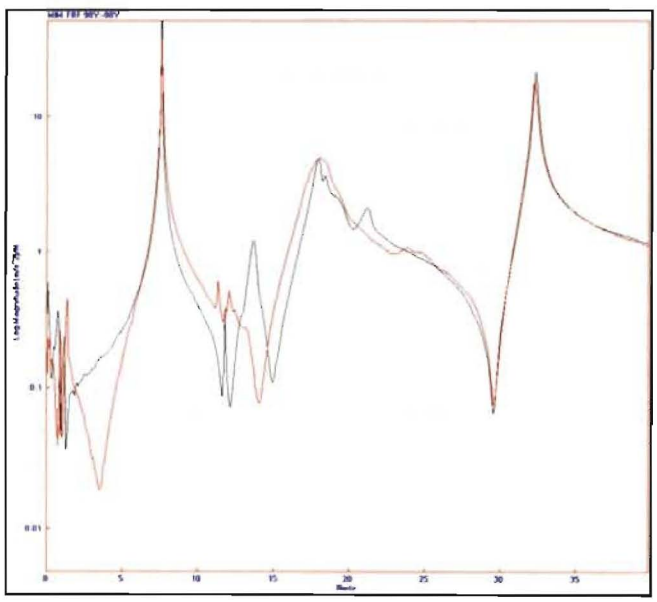

Figure 17: FRF comparison between stiffened baseline (black) and stiffened 5 meter (red) configurations

Comparison of the two FRFs shows minimal difference at the first and third flap-wise modes, but a noticeable difference at the second flap-wise mode. A possible explanation for this difference is the same as when moving the frame outboard; a change in the interaction of the lead-lag mode with the second flap-wise bending mode. Table 11 is a comparison of the frequencies for the first three flap-wise modes.

Table 11: Comparison of Natural Frequencies for the Stiffened Baseline and Stiffened 5 Meter Configurations

	Stiffened Baseline Configuration (Hz)	Stiffened 5 Meter Configuration (Hz)	Percent Difference
First Flap-wise	7.6	7.6	0
Second Flap-wise	21.2	18.4	13.21
Third Flap-wise	32.3	32.3	0

Test 6: Stiffened Frame Moved to 3 Meters from Root

Although the best position for the supports would be at the node of a mode, a test to determine the effects of moving the tip-end support further inboard, near the center of gravity (CG) of the blade was performed. Accordingly, the frame was moved to 3 meters from the root, Figure 18. Note that the strap contact area is significantly increased because of the much larger chord in this region of the blade, and the effects of strap contact are going to be greater for this configuration. In this test, the strap was in contact with the low-pressure (LP) side of the blade. The resulting FRF overlay is shown in Figure 19.

Figure 18: Tip-end frame in baseline location 6.5m from root (left) versus moving the frame to 3m from root (right)

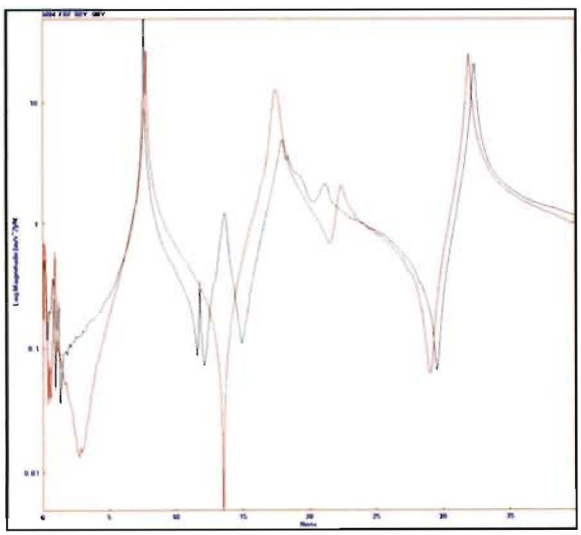

Figure 19: FRF comparison between stiffened baseline and stiffened 3 meter, LP-side contact configurations

Comparison of the two FRFs shows noticeable difference at all three modes. A possible explanation for this difference is due to the blade being substantially cantilevered in this configuration, which would change the frequencies. The extensive contact between the blade surface and the tip end support sling would have an effect on the frequencies and mode shapes as well. Table 12 is a comparison of the frequencies for the first three flap-wise modes.

Table 12: Comparison of Natural Frequencies for the Stiffened Baseline and 3 Meter, LP-Side Contact Configurations

	Stiffened Baseline Configuration (Hz)	Stiffened 3 Meter, LP-Side Contact Configuration (Hz)	Percent Difference
First Flap-wise	7.6	8.15	6.75
Second Flap-wise	21.2	22.1	4.07
Third Flap-wise	32.3	32.1	0.62

Test 7: Changing Support Sling Contact with Blade Surface

With the tip end support located near the CG of the blade the sling has substantial contact with the blade surface. Rotating the blade drastically changes which surfaces (low-pressure or high-pressure) are in contact with the sling and the amount of contact. To test this effect, two measurements were taken, one with the blade rotated such that the sling was in contact with much of the low-pressure side and another where the blade was centered in the sling and the contact was roughly equal on both the low-pressure and high-pressure sides, Figure 20. All support frames were stiffened. The resulting FRF overlay is shown in Figure 21.

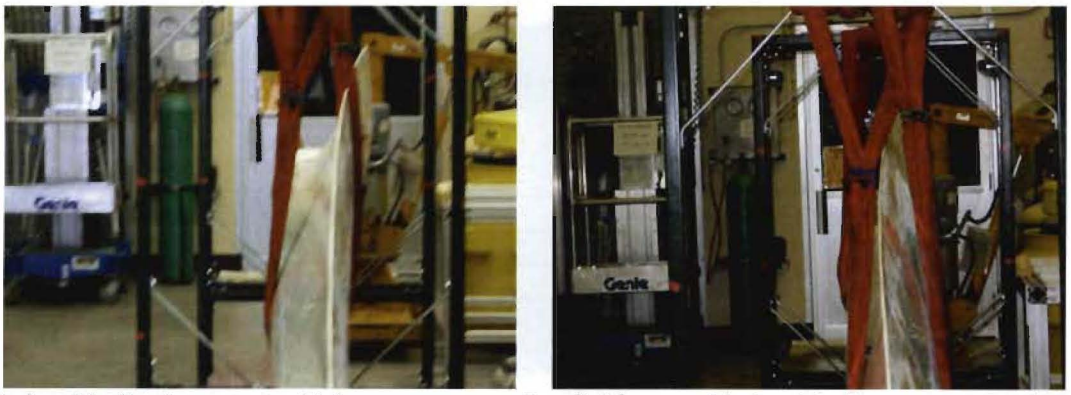

Figure 20: Blade with sling in contact with low-pressure surface (left) versus blade with sling contact equal on both sides (right)

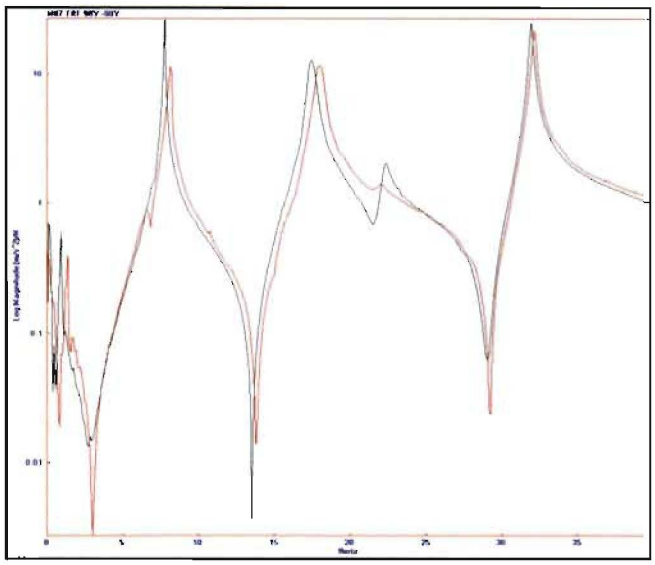

Figure 21: FRF comparison between low-pressure side contact (black) and equal side contact (red) configurations

Comparison of the two FRFs shows noticeable difference at all three modes, particularly with the first and second modes. The difference is likely due to the drastic difference in surface contact scenarios changing the interaction between the blade and the tip-end support. Table 13 is a comparison of the frequencies for the first three flap-wise modes.

Table 13: Comparison of Natural Frequencies for the Low-Pressure Side Contact and Equal Side Contact configurations

	Low-Pressure Side Contact Configuration (Hz)	Equal Side Contact Configuration (Hz)	Percent Difference
First Flap-wise	7.78	8.15	4.54
Second Flap-wise	22.4	22.1	1.35
Third Flap-wise	32.0	32.1	0.31

Test 8: Root Support Moved to 0.86 Meters

Although most of the testing was focused on the location of the tip end frame, the effect of the root support was also examined. The support was moved outboard to 0.86m from the root (originally at 0.57m), Figure 22. The resulting FRF overlay is shown in Figure 23, where the black trace is the baseline measurement with the stiffened frame with both the tip and root end supports at the original locations, and the red trace is the measurement after moving the root support outboard.

Figure 22: Root support in baseline location (left) versus moved to 0.86m from root (right)

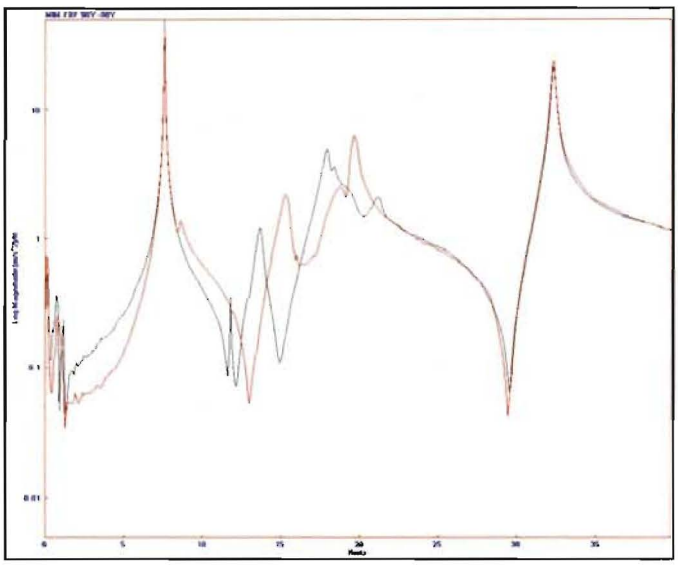

Figure 23: FRF comparison between stiffened baseline (black) and shifted root (red) configurations

Comparison of the two FRFs shows minimal difference at the first and third flap-wise modes, but a noticeable difference at the second flap-wise mode. Table 14 is a comparison of the frequencies for the first three flap-wise modes.

Table 14: FRF Comparison of Natural Frequencies for the Stiffened Baseline and Shifted Root Configurations

	Stiffened Baseline Configuration (Hz)	Shifted Root Configuration (Hz)	Percent Difference
First Flap-wise	7.6	7.6	0
Second Flap-wise	21.2	19.7	7.08
Third Flap-wise	32.3	32.3	0

Appendix B: Nonlinear Study

B.1 Nonlinear Testing in Fixed-Free Configuration

In order to determine the existence of significant nonlinearities on the blade system, a nonlinear study was performed. The nonlinear study included a reciprocity check and a varied force impact test. The blade was in the Fixed-Free configuration for this testing.

B.1.1 Varied Impact Force Test

The FRF, $H(j\omega)$, is calculated by normalizing the autopower spectrum of the response by the input force spectrum. For a linear sytem, the FRF is independent of the impact force applied, and the same FRF is obtained regardless of the impact force.

To test if the system is linear and therefore independent of the force applied, drive point measurements at point 78 on the blade with varying impact forces were recorded. The FRFs were then compared to see if there was no difference, and therefore the system was linear, or if there were differences in magnitude or frequency, and therefore the system was nonlinear.

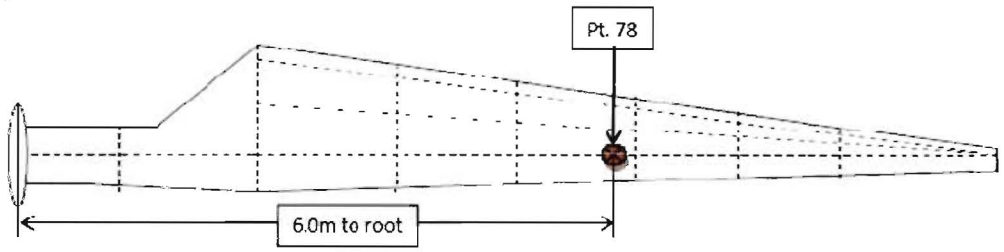

Figure 24: Layout of impact and measurement point on CX-100

Table 15: Frequencies and Magnitudes at First Six Modes

Impact	1st Flap-wise		1st Lead-Lag		2nd Flap-wise	
Force (N)	Freq (Hz)	Mag (m/s2)	Freq (Hz)	Mag (m/s2)	Freq (Hz)	Mag (m/s2)
250	3.2	1.76	4.21	0.0692	8.79	0.893
330	3.2	1.38	4.21	0.0635	8.79	0.912
396	3.2	1.42	4.21	0.0642	8.79	0.942
438	3.2	1.59	4.21	0.0632	8.79	0.969
510	3.2	1.49	4.21	0.0604	8.79	0.986

Impact	2nd Lead-Lag		3rd Flap-wise		4th Flap-wise	
Force (N)	Freq (Hz)	Mag (m/s2)	Freq (Hz)	Mag (m/s2)	Freq (Hz)	Mag (m/s2)
250	16.8	0.749	19.2	0.424	30.9	2.97
330	16.8	0.735	19.1	0.422	30.9	2.97
396	16.8	0.73	19.1	0.438	30.9	2.94
438	16.8	0.728	19.1	0.436	30.9	2.91
510	16.8	0.71	19.1	0.427	30.9	2.96

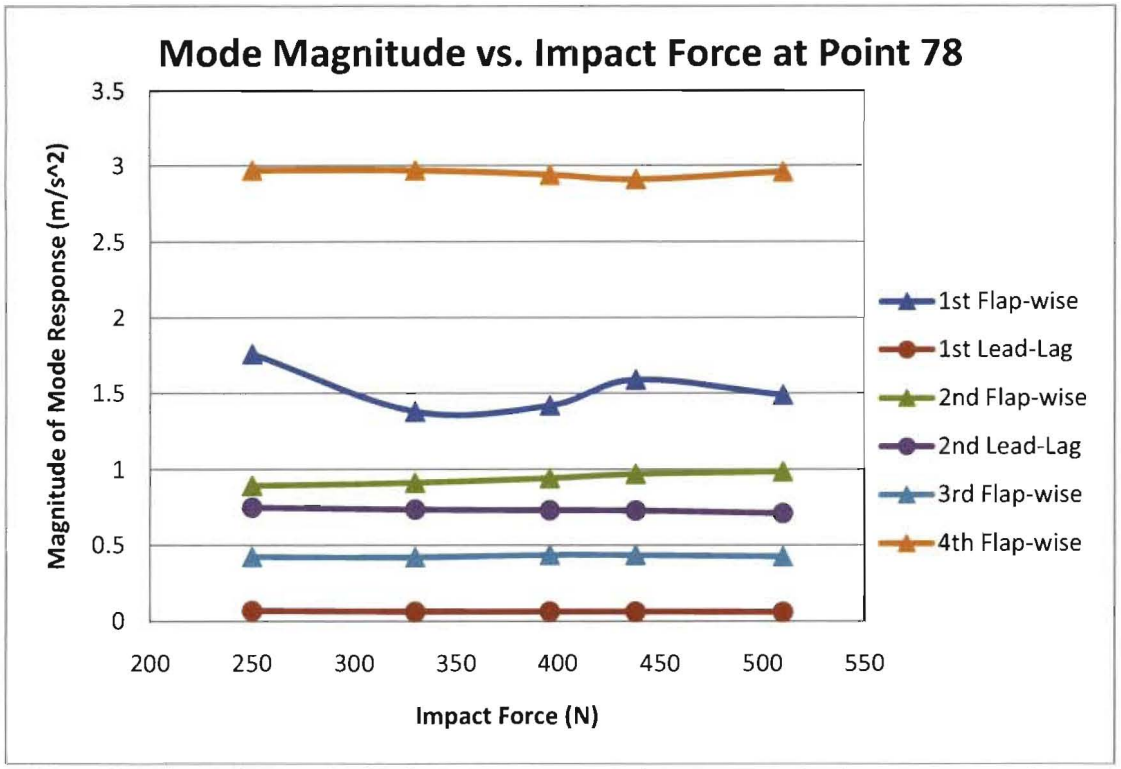

Figure 25: Change in magnitude of response at various low-order modes based on impact force

For each of the six modes analyzed, the frequencies did not change based on the impact force. However, the magnitudes of some modes varied depending on the impact force, with no deterministic patterns emerging. The first, second and fourth flap-wise modes, in particular, exhibit some change in the magnitude of response for different impact forces whereas the third flap-wise mode shows little change. The two lead-lag modes had little change in response magnitude for the changes in impact force. The existence of some fluctuation in the system response magnitude at differing impact forces may be indicative of nonlinearity in the system.

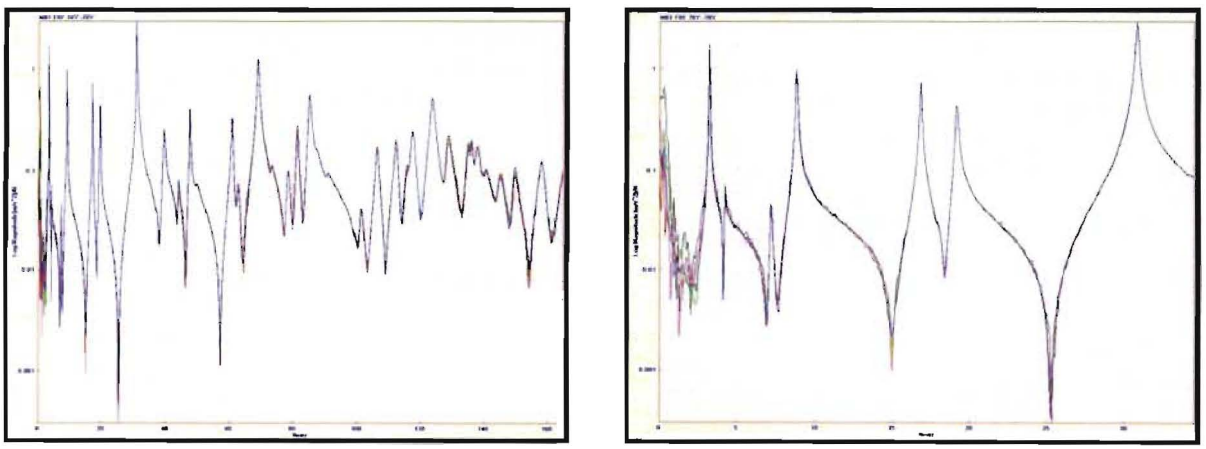

Figure 26: All impacts (250 to 510N) FRF overlay plot, showing a frequency range of zero to 160Hz (left) and zoom in of zero to 35Hz (right)

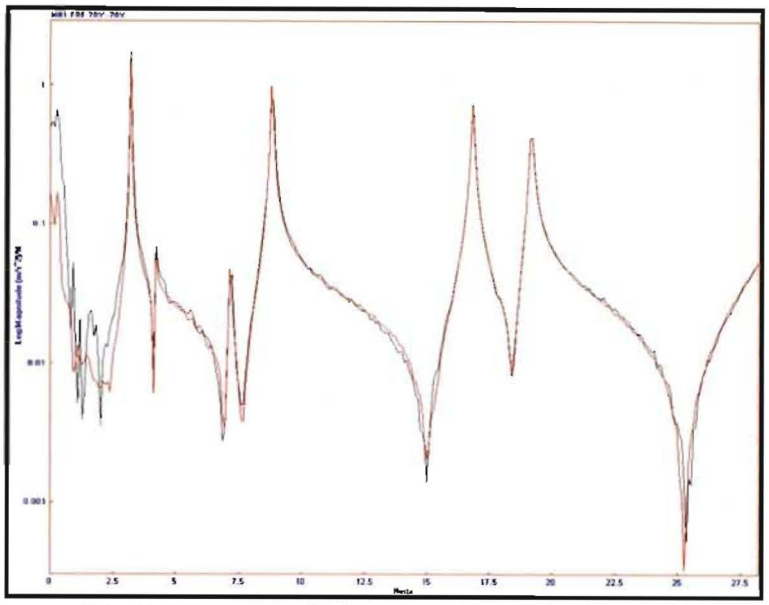

Figure 27: Lowest force impact (black) 250N, versus highest force impact (red) 510N, showing first five modes, zero to 28Hz

B.1.2 Reciprocity Test

The linear reciprocity assumption was tested by impacting at point 78 and measuring at point 91 versus impacting at 91 and measuring at 78. With a perfectly linear system, the FRF will be exactly the same for either scenario. If the system is nonlinear, the FRF from impacting at 91 and impacting at 78 may have different mode frequencies and/or magnitudes.

The same accelerometer was used to measure at both points and care was taken to measure and impact in the same spot for each point. Accelerometer used: PCB 352A24, S/N 39148. One impact and one measurement collected (no averaging). Impact at point 78 was force of 307N. Impact at point 91 was force of 220N

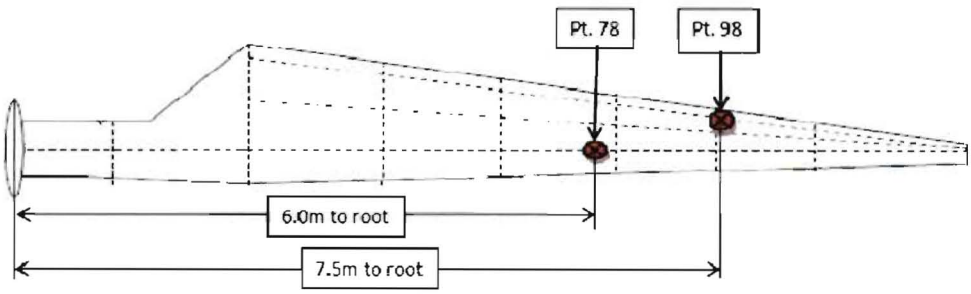

Figure 28: Layout of impact and measurement points on CX-100

Table 16: Frequencies and Magnitudes at First Six Modes, Comparing Impacting at Point 91 (Red) with Impacting at 78 (Blue)

			1st Flap-wise		1st Lead-Lag		2nd Flap-wise	
Measure @:	Impact @:	Impact Force (N):	Freq (Hz)	Mag (m/s2)	Freq (Hz)	Mag (m/s2)	Freq (Hz)	Mag (m/s2)
78	91	220	3.2	2.45	4.21	0.156	8.79	0.731
91	78	307	3.2	2.22	4.21	0.112	8.79	0.798
% Diff. Measure @78 vs. Measure @91			0%	9%	0%	28%	0%	-9%
			2nd Lead-Lag		3rd Flap-wise		4th Flap-wise	
Measure @:	Impact @:	Impact Force (N):	Freq (Hz)	Mag (m/s2)	Freq (Hz)	Mag (m/s2)	Freq (Hz)	Mag (m/s2)
78	91	220	16.8	1.11	19.1	1.21	30.9	4.32
91	78	307	16.8	1.25	19.2	1.15	30.9	4.46
% Diff. Measure @78 vs. Measure @91			0%	-13%	-1%	5%	0%	-3%

For the first several modes, there is no shift in frequency based on the impact or measurement location. The magnitudes at those frequencies are not perfectly consistent, with the lead-lag mode magnitudes having more variance between impacting at point 91 versus impacting at point 78. This greater difference is likely because impacts and measurements were only in the Y-axis, which is normal to the lead-lag direction and thereby not exciting or measuring the lead-lag modes. The flap-wise modes show less difference between impacting at one point versus the other. This difference may be negligible if multiple samples are taken and averaged, as only one impact for each measurement scenario was recorded.

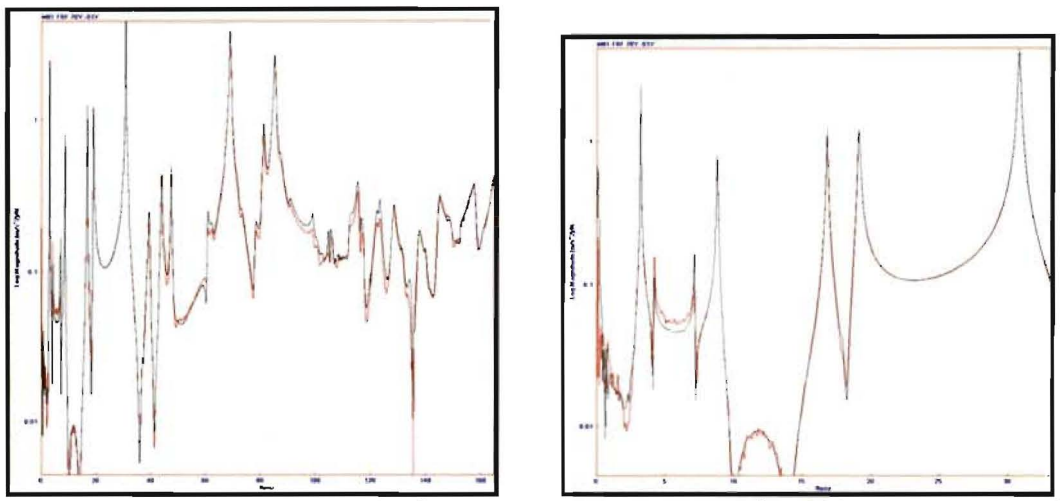

Figure 29: FRF overlay, impacting at point 91 (red) versus impacting at point 78 (black) from 0 to 160Hz and zoomed in from 0 to 30Hz

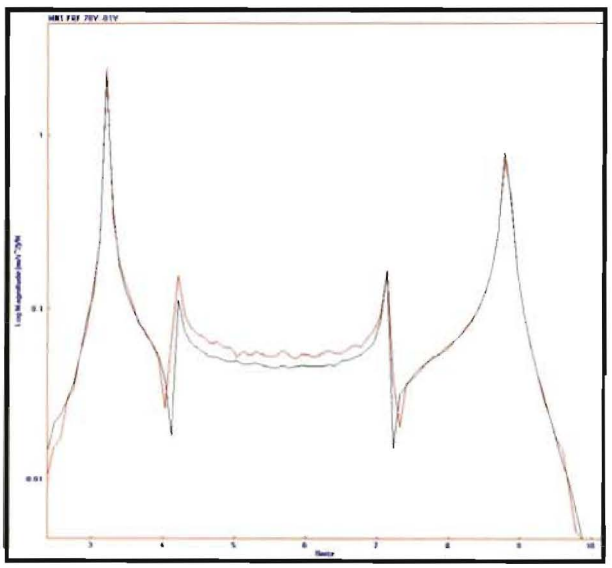

Figure 30: FRF overlay showing first 3 modes (3.2 Hz, 4.21 Hz, 8.79 Hz), impacting at 91 (red) versus impacting at 78 (black) from 0 to 10 Hz

After analyzing the data from the reciprocity check and the varied force impact test, nonlinearities were observed to be present in the system. In the future, further study may be needed to determine the nonlinear effects on the assumption of linearity for the purposes of modal testing.

Appendix C: Structural Health Monitoring Study

In order for SHM to be a viable method, variation should come from damage, rather than day-to-day conditions. Testing was done to determine the variation between tests on the same day, as well as between different days.

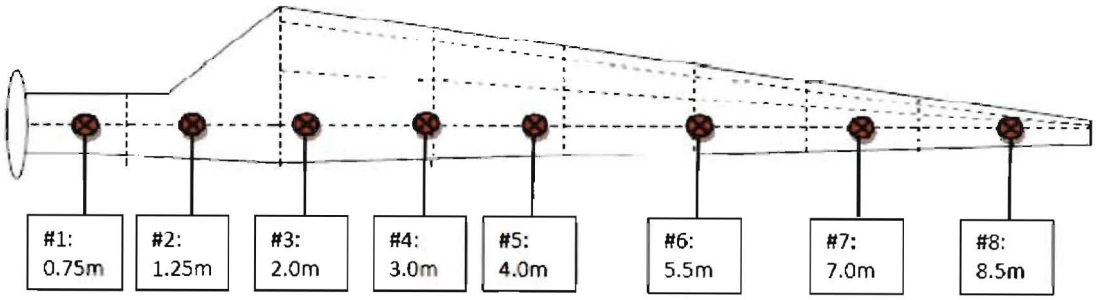

Figure 31: Sensor MFC patch locations on blade centerline

C.1 Same-Day Repeatability Test

Before studying any variations due to environment or loading, verification of repeatability between tests needed to be established. Accordingly, both the chirp and burst random excitations were applied twice for each measurement point. Figure 32 shows a FRF overlay of the chirp and burst random responses at point 1 with the first test in black and the second test in blue.

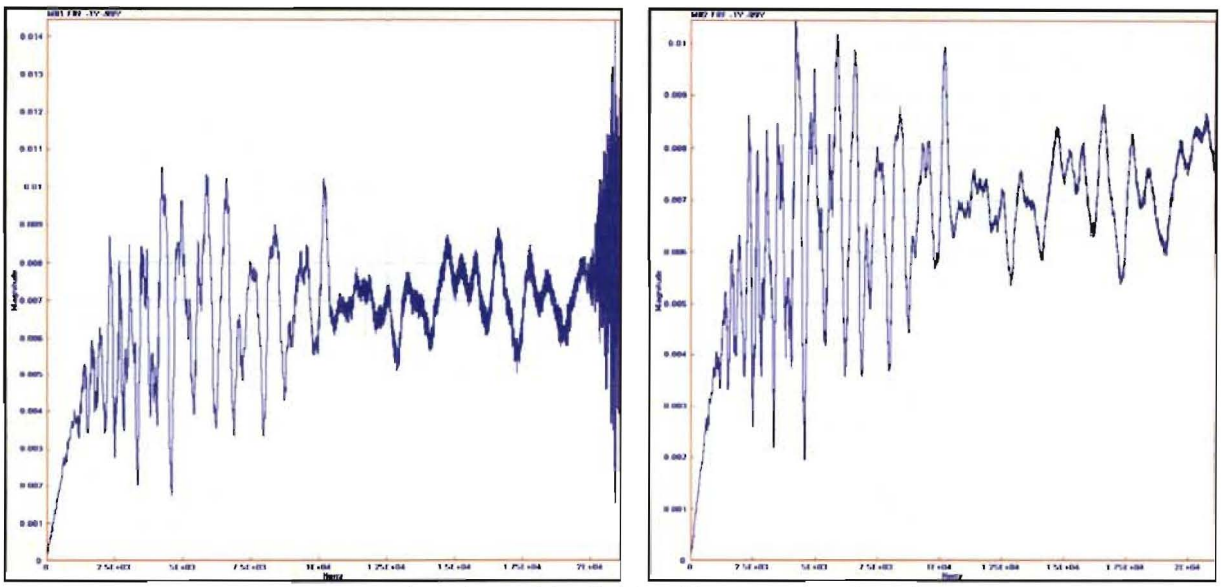

Figure 32: FRF overlay of sine chirp (left) and burst random (right) responses at point 1

The FRF overlay indicates that there is high repeatability between tests as the two traces are almost perfectly overlaid on top of each other. Accordingly, any variation in SHM results will not be due to the issue of repeatability with the same environmental and loading conditions. In addition, both excitation techniques experience the same repeatability, with identical responses up to 10 kHz.

C.2 Different Days Repeatability Test

Although important to establish repeatability between tests, equally important is the day to day repeatability. Since environmental conditions change frequently for wind turbines, there needs to be an awareness of the

effect of the environment on SHM results. Accordingly, the FRF at point 1 due to a burst random excitation is compared across four days of testing in Figure 33, where each color line corresponds to a temperature on a different day (Red = 78.7°F, Blue = 75.7 °F, Green = 74.6 °F, Purple = 75.5 °F).

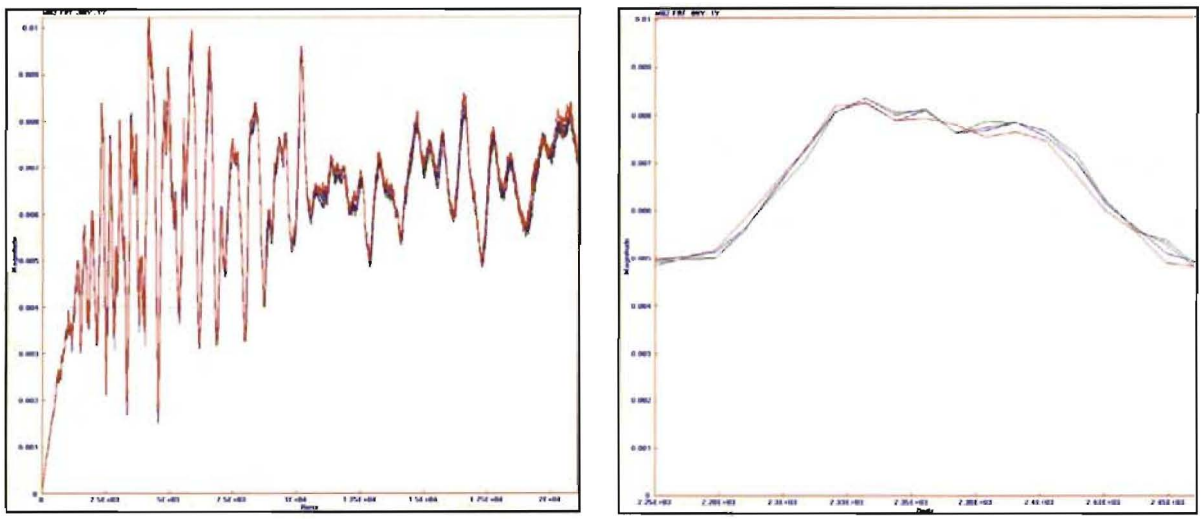

Figure 33: Comparison of temperature range over entire frequency range (left) and zoom in for one peak (right)

The FRF overlay indicates that there is high repeatability between tests as there is minimal variation. Further study may be needed to determine if the variation increases as the blade experiences a wider temperature range.

C.3 Effective Frequency Determination Test

Low frequency waves have a long wavelength, allowing them to travel substantially farther than high frequency waves. High frequency waves, however, are able to detect much smaller defects. Accordingly, for various sensor locations on the blade, there needs to be an awareness of the maximum frequency range at which a useable signal is measured. Figure 34 contains a comparison of the responses at points 4 and 8 with a burst random excitation where the black response is for point 4, and the blue response is for point 8.

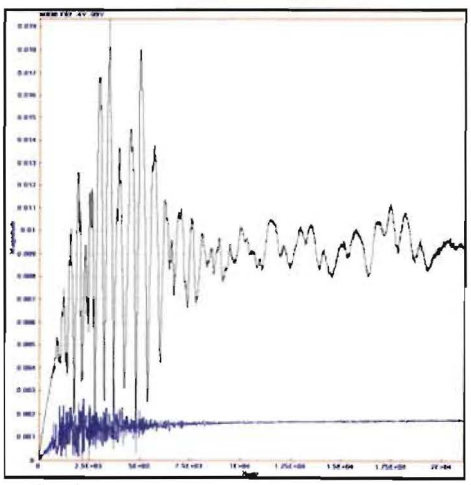

Figure 34: FRF overlay between points 4 and 8 for burst random excitation

While the response at point 4 contains a high signal to noise ratio across the entire frequency range, the response at point 8 contains noise at all frequencies. Comparing the responses at all 8 points yields Table 17 which summarizes the effective frequency for each point.

Table 17: Effective Frequency for Points on Blade

Point	1	2	3	4	5	6	7	8
Effective Frequency (kHz)	0-20	0-20	0-20	0-20	5-20	5-20	5-20	5-20

The points located in the structural region have a measurable response across the entire frequency range. In comparison, the points located in the aerodynamic region experience a rapid drop in effective frequency as the distance from the actuator increases. In addition, the time signal also shows a drop off in amplitude due to the decreasing energy transferred to the sensor, as shown in Figure 35, where red = point 3, black = point 4, orange = point 5 and green = point 6 for a burst random input.

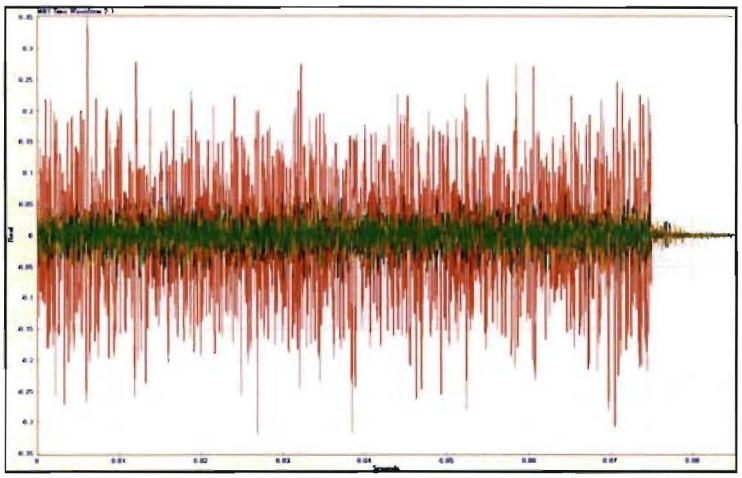

Figure 35: Comparison of time signal responses for points 3, 4, 5, and 6

C.4 Preload Test

In addition to temperature variation, wind turbine blades experience significant variation in loads. Since SHM needs to distinguish damage from load variation, a study of the effect of loading on the blade was performed. With the blade in the fixed-free configuration, various displacements at the tip were applied upward in the vertical direction to simulate an operational load that might change the response. Figure 36 is a FRF overlay for a random signal response at point 1, with the green line the baseline, the black line 1 inch, and the red line 1.5 inches of tip displacement, bending the blade in the lead-lag direction.

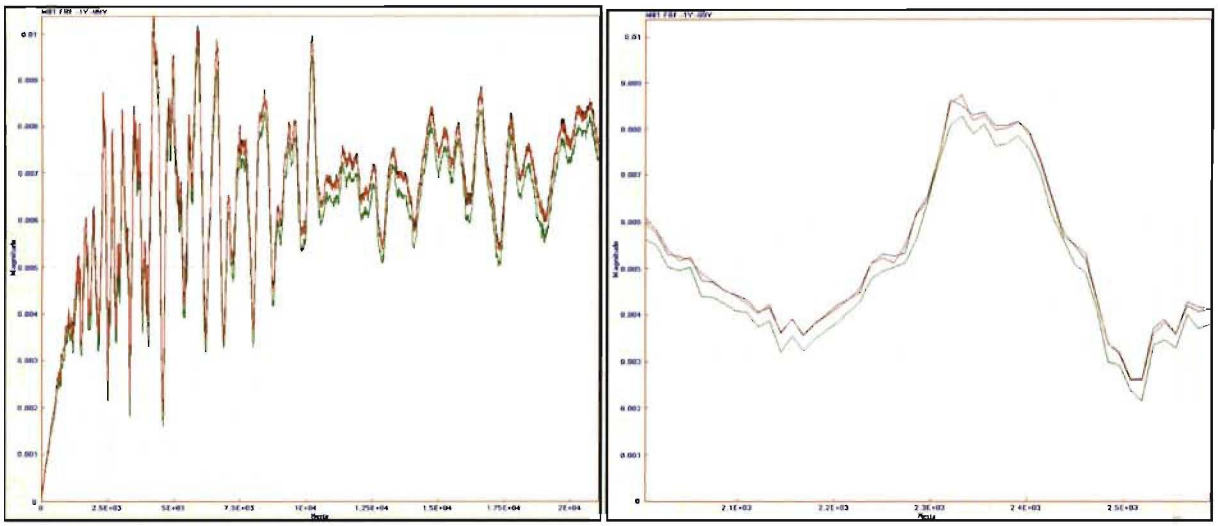

Figure 36: Comparison of preloads over entire frequency range (left) and zoom in for one peak (right)

As shown, the addition of the preload does not have an effect on the frequency peaks. The magnitude, however, is noticeably changed by the preload, and further study will be needed to determine a way to detect damage with the changing operational loads.